sustainability

MDPI

Article

Chitosan-Based Nanocomposite for Tetracycline Removal

Gergana Kirova [1,*], Margarita Stoytcheva [2], Zdravka Velkova [1], Georgi Avdeev [3], Nikolay Zahariev [4] and Velizar Gochev [5]

[1] Department of Chemical Sciences, Faculty of Pharmacy, Medical University of Plovdiv, 4000 Plovdiv, Bulgaria
[2] Independent Researcher, 4000 Plovdiv, Bulgaria
[3] Laboratory of X-Ray Diffraction Methods and Computed Tomography, Institute of Physical Chemistry, Bulgarian Academy of Sciences, 1113 Sofia, Bulgaria
[4] Department of Pharmaceutical Technology and Biopharmacy, Faculty of Pharmacy, Medical University of Plovdiv, 4000 Plovdiv, Bulgaria
[5] Department of Biochemistry and Microbiology, Faculty of Biology, "Paisii Hilendarski" University of Plovdiv, 4000 Plovdiv, Bulgaria
* Correspondence: gergana.kirova@mu-plovdiv.bg

Abstract

The presence of antibiotic residues in aquatic environments poses a significant risk to water quality and public health, creating a need for effective and sustainable treatment technologies. In this study, a chitosan-based nanocomposite containing silver, cobalt, and iron (CS-HNC) was synthesized under mild conditions without a calcination step and evaluated for the removal of tetracycline (TC) from aqueous solutions. Attention was given to TC removal at an initial concentration of 10 mg L^{-1}. Although this concentration exceeds those typically reported for natural surface waters, it is lower than the concentrations frequently employed in adsorption studies and therefore provides a useful basis for evaluating the performance of the developed adsorbent under controlled laboratory conditions. The material was characterized by field-emission scanning electron microscopy (FE-SEM), energy-dispersive X-ray spectroscopy (EDS), X-ray diffraction (XRD), high-resolution transmission electron microscopy (HRTEM), and Fourier transform infrared spectroscopy (FTIR). The characterization results confirmed the successful formation of the nanocomposite and the incorporation of metal-containing phases within the chitosan matrix. The effects of key sorption parameters were investigated, showing that TC removal was only weakly influenced by pH and ionic strength. The maximum sorption capacity reached 45.7 mg g^{-1}, while removal efficiencies of 94.3% and 98.4% were achieved after 30 and 120 min, respectively, at an initial TC concentration of 10 mg L^{-1}. Sorption kinetics were best described by the pseudo-second-order model, whereas equilibrium data were better fitted by the Freundlich isotherm model. No detectable leaching of Ag, Co, or Fe was observed after soaking the material in deionized water and in a solution adjusted to pH 2 for 24 h, indicating good stability of the synthesized material under the investigated conditions. These findings suggest that the developed CS-HNC nanocomposite is a promising sorbent for the removal of TC.

Keywords: tetracycline; sorption; nanocomposite; wastewater treatment

Check for updates

Academic Editor: Andreas N. Angelakis

Received: 13 August 2026
Revised: 10 October 2026
Accepted: 11 October 2026
Published: 14 October 2026

Copyright: © 2026 by the authors. Licensee MDPI, Basel, Switzerland. This article is an open access article distributed under the terms and conditions of the Creative Commons Attribution (CC BY) license.

1. Introduction

Tetracyclines are among the most widely used antibiotics in human and veterinary medicine, aquaculture, and livestock production, where they are used as growth promoters. Their low production costs, high efficiency, and broad antimicrobial activity have

contributed to their widespread use that ranges from treating serious conditions like pneumonia or prevention of malaria to treatment of acne [1–4]. Their wide application is also due to their antimicrobial properties, low toxicity, and activity against a broad spectrum of microorganisms [1,2].

Tetracyclines' extensive use makes them among the most frequently produced antibiotics worldwide, with China being the leading producer [2–4]. Despite growing concerns regarding the development of antimicrobial resistance, tetracyclines continue to be widely used because they are effective against Gram-positive and Gram-negative bacteria, as well as other microorganisms such as chlamydia, mycoplasmas, rickettsia, and protozoan parasites [1].

Among the tetracyclines, tetracycline (TC) is one of the most frequently detected antibiotics in aquatic environments. Following administration, approximately 80% of TC is excreted in urine and feces, often in its biologically active form [1,2,4]. As a result, significant amounts of TC enter wastewater treatment systems and are subsequently released into natural aquatic environments [5–10].

Different strategies have been developed to degrade or remove TC from wastewater, including enzymatic degradation [3], ozonation [5], photo-Fenton oxidation [6], microbial biodegradation [7], photolysis [9], and adsorption-based approaches [8,10–14]. All these techniques have drawbacks such as the formation of toxic by-products, incomplete degradation of the antibiotic, sludge generation, high energy consumption, and high operational costs [2].

Among the available treatment methods, adsorption has attracted considerable attention because of its operational simplicity, versatility, and effectiveness in removing antibiotics from aqueous solutions. Compared with many degradation-based technologies, adsorption does not require specialized reaction conditions and can often be implemented using renewable and regenerable sorbent materials. Recent studies continue to identify adsorption as one of the most promising approaches for the removal of TC and related antibiotics from water and wastewater [10–14]. Nevertheless, conventional sorbents are not completely effective for TC removal, which contributes to the continued detection of TC residues in surface and drinking water sources [2,3].

The permanent presence of TC in the environment can cause serious ecological disturbances, promote the development of antibiotic-resistant bacteria, and pose potential risks to public health. Therefore, the development of efficient and environmentally friendly sorbent materials remains an important research priority and a major focus of current research [3].

In recent years, increasing attention has been given to sustainable and green materials for water purification, particularly those derived from natural or renewable sources. New and environmentally friendly adsorbents for TC removal have been synthesized from waste PET bottles [9], mineral and clay-based materials [10], silica-based adsorbents [11], nanocomposites [13,14], and biopolymer-based materials and their composites [8,15,16].

Recent reviews have highlighted the growing interest in biopolymer-based materials for antibiotic removal because of their tunable surface chemistry, biocompatibility, biodegradability [8,15], and capacity for further modification with metal-containing phases and other functional materials [17,18]. The development of such materials aligns with the principles of sustainable chemistry and circular economy, aiming to reduce environmental impact while maintaining high treatment efficiency [8,15,16].

Chitosan (CS) is the deacetylated derivative of chitin, and it is the second most abundant natural polymer in the world [15]. CS is produced from chitin-rich crustacean shell waste, a by-product of the seafood industry that can be transformed into a valuable and sustainable material. Its environmentally friendly nature, together with its biodegradability, biocompatibility, non-toxic behavior, and antimicrobial activity, has promoted its extensive

application in environmental protection and water treatment processes [8,15,16]. Various biopolymer-based materials, including nanoparticles, hydrogels, films, and nanocomposites, have been widely investigated for applications in medicine, biotechnology, and wastewater treatment [8,15,16].

TC molecules can interact with a variety of metal-containing surfaces and are known to form complexes with numerous metal ions, including Mg(II), Cu(II), Ca(II), Fe(II), Fe(III), Ni(II), Co(II), Al(III), Pb(II), and Mn(II), which may enhance sorption interactions with metal-containing sorbents [19,20]. Incorporation of metal oxide nanoparticles into a chitosan matrix can improve sorption performance by providing additional active sites, enhancing surface area, and facilitating additional interactions between the adsorbent and contaminant molecules [17,18,21–24].

Despite the considerable progress achieved in the development of chitosan-based adsorbents, relatively few studies have investigated the simultaneous incorporation of Ag-, Co-, and Fe-containing phases within a chitosan matrix using a single-step synthesis strategy [21,23]. In many reported systems, metal-containing nanoparticles are synthesized separately and subsequently immobilized onto the polymer support, resulting in more complex preparation procedures [21–24]. Therefore, the development of multifunctional chitosan-based composites that can be prepared under mild conditions without high-temperature calcination remains of considerable interest [13,14,16]. Preliminary experiments conducted during material development demonstrated that incorporation of Fe ions into chitosan improved TC removal compared with unmodified chitosan but was accompanied by partial Fe release under the investigated conditions. This observation motivated the incorporation of Co and Ag into the chitosan matrix.

The novelty of the present work lies in the synthesis of an Ag-Co-Fe modified chitosan nanocomposite, hereafter referred to as the chitosan hybrid nanocomposite (CS-HNC), using a simple one-step coprecipitation method performed under mild conditions without high-temperature calcination. Unlike many previously reported metal-modified chitosan materials, in which metal-containing nanoparticles are synthesized separately and subsequently incorporated into the polymer matrix, the metal-containing phases in the present study were generated directly within the chitosan matrix during composite formation. This approach simplifies the synthesis procedure and reduces energy requirements. The preparation of CS-HNC was carried out in aqueous media at a relatively low temperature (50 °C) and without high-temperature calcination, making the synthesis route comparatively simple and less energy-intensive than many reported metal-containing nanocomposite adsorbents.

The objectives of this study were to evaluate the adsorption performance of the developed CS-HNC toward TC and to investigate the influence of key operational parameters, such as solution pH, adsorbent dosage, contact time, initial TC concentration, and ionic strength, on the adsorption process.

2. Materials and Methods

2.1. Reagents

The reagents used in the study are summarized in Table 1.

A TC stock solution with a concentration of 200 mg L^{-1} was prepared daily with deionized water. Working solutions were prepared with an adequate dilution of the stock TC solution.

2.2. Preparation of the Chitosan Hybrid Nanocomposite (CS-HNC) Sorbent

The CS-HNC was prepared using a modified co-precipitation method based on previously reported procedures [17,21–25].

Table 1. Chemicals and reagents used in the study.

Reagent	Formula	Purity/Specification
Tetracycline hydrochloride (TC)	$C_{22}H_{24}N_2O_8 \cdot HCl$	≥95%, HPLC assay
Iron(III) nitrate nonahydrate	$Fe(NO_3)_3 \cdot 9H_2O$	99.0–101.0%, ACS, Reag. Ph. Eur.
Cobalt(II) nitrate hexahydrate	$Co(NO_3)_2 \cdot 6H_2O$	≥98%
Silver nitrate	$AgNO_3$	≥99.0%, ReagentPlus®
Chitosan (high molecular weight)	—	DD >75%
Sodium hydroxide	NaOH	≥97.0%
Nitric acid	HNO_3	70%, ACS reagent
Hydrochloric acid	HCl	37%, ACS reagent
Sodium chloride	NaCl	≥99.5%, ACS, Reag. Ph. Eur.
Ethanol	C_2H_5OH	96%, ACS, Reag. Ph. Eur.
Acetic acid (glacial)	CH_3COOH	≥99.7%, ACS, Reag.
Potassium nitrate	KNO_3	≥99.0%, ACS reagent

All reagents were purchased from Sigma-Aldrich (Merck KGaA, Darmstadt, Germany). Deionized water produced by an ELGA PURELAB Chorus 2 purification system was used for solution preparation.

Briefly, 0.403 g of $Fe(NO_3)_3 \cdot 9H_2O$, 0.145 g of $Co(NO_3)_2 \cdot 6H_2O$, and 0.126 g of $AgNO_3$ were dissolved in 100 mL of 2% (*v*/*v*) CH_3COOH. Subsequently, 1 g of chitosan was added to the metal solution, and the mixture was placed on a magnetic stirrer with heating. The solution was vigorously stirred at 400 rpm and 60 °C until the chitosan was completely dissolved and a homogeneous gel was formed.

While still warm, the viscous solution was transferred into a syringe with a 2 mm internal tip diameter and extruded dropwise into 0.5 M NaOH solution. The formed spheres were kept in the NaOH solution for 30 min, allowing simultaneous chitosan solidification and metal hydroxide co-precipitation within the polymer matrix. The obtained CS-HNC spheres were black in color. The spheres were filtered and washed repeatedly with deionized water until a neutral pH of the filtrate was reached. Then the metal-containing nanocomposite spheres were only dried at 50 °C for 24 h, without the high-temperature calcination of 400–800 °C typically required in conventional ferrite nanoparticle synthesis.

2.3. Characterization of the CS-HNC

The morphology of the CS-HNC was examined by FE-SEM (Tescan LYRA 3 (Tescan, Brno, Czech Republic)) operated at an accelerating voltage of 10 kV with a backscattered electron detector. The EDS analysis was performed using Bruker XFlash 6I30 (Bruker, Billerica, MA, USA). The samples were prepared by placing a 1 mm thick layer on double-sided conductive carbon tape. The measurements were carried out at an accelerating voltage of 10 kV and a working distance of 9 mm.

The XRD analysis was performed using an Empyrean X-ray Diffractometer (PANalytical, Almelo, The Netherlands) equipped with a PIXcel3D detector (PANalytical, Almelo, Netherlands). The measurements were carried out using Cu Kα radiation (λ_1 = 1.5406 Å, λ_2 = 1.5444 Å) generated at 40 kV and 30 mA. The diffraction patterns were recorded in the 2θ range from 3° to 60° with a step size of 0.053° and a counting time of 93.33 s per step. Measurements were carried out at room temperature using a flat sample holder without sample spinning. The relatively long counting time ensured a high signal-to-noise ratio and improved detection of weak diffraction peaks.

The morphology and microstructure of the CS-HNC sorbent were investigated by HRTEM (TalosF200C, Thermo Scientific, Waltham, MA, USA). For HRTEM analysis, the samples were dispersed in ethanol, ultrasonicated, deposited onto carbon-coated copper grids, and dried at room temperature. Measurements were performed at 200 kV,

and particle size distributions were determined from at least 100 nanoparticles. Analyses were conducted before and after TC sorption to evaluate morphology, size, and aggregation behavior.

An ATR-FTIR spectrometer (PerkinElmer Frontier FTIR Spectrometer, PerkinElmer, Waltham, MA, USA) was used to record the FTIR spectra of the composite before and after TC sorption. The spectra were collected in the range 4000–400 cm^{-1} at a resolution of 4 cm^{-1} with 32 scans.

The solid addition method [25] was used to determine the point of zero charge (pHpzc) of the nanocomposite. For this purpose, KNO_3 solutions with different initial pH values (pH_i = 2–10) were prepared by adjusting the pH with 0.1 mol L^{-1} HNO_3 or 0.1 mol L^{-1} NaOH. Subsequently, 100 mL of each solution was transferred into Erlenmeyer flasks containing 1 g of CS-HNC sorbent. The flasks were agitated for 48 h at room temperature, and the final pH (pH_f) of the solutions was measured using a calibrated pH meter (WTW inoLab pH 7310 equipped with a WTW SenTix precision pH electrode, Xylem, Washington, DC, USA).

The difference between the initial and final pH values ($\Delta pH = pH_i - pH_f$) was plotted against pH_i. The pHpzc corresponds to the point where $\Delta pH = 0$ (where the curve intersects the *x*-axis).

2.4. Sorption Experiments

Batch sorption experiments were performed to investigate the influence of different parameters on the TC removal and uptake, including initial pH of the solution (3–9), amount of sorbent (25–150 mg), contact time (0–120 min), initial TC concentration (10–100 mg L^{-1}), and ionic strength.

The batch experiments were carried out in 25 mL stoppered Erlenmeyer flasks at 25 °C on a magnetic stirrer at 150 rpm. To prevent photodegradation of TC, all sorption vessels were wrapped with aluminum foil. A blank sample containing only the TC solution was included in each experimental series. All experiments were performed in triplicate, and the results are reported as mean values. The reproducibility of the adsorption measurements was satisfactory, with relative standard deviation (RSD) values generally below 5%. For example, at an initial TC concentration of 10 mg L^{-1}, the adsorption capacity was 3.13 ± 0.10 mg g^{-1} (95% confidence interval, n = 6), corresponding to an RSD of 2.97%.

After the sorption process, the residual TC concentration was determined using a UV–visible spectrophotometer (Ultrospec 3300 Pro, Amersham Biosciences, Amersham, UK) at 355 nm. For samples containing very low residual TC concentrations, particularly in experiments yielding adsorption efficiencies above 90%, a 5 cm quartz cuvette was employed.

The removal efficiency (*R*, %) was calculated using the following equation:

$$R(\%) = \frac{C_i - C_f}{C_i} \times 100 \quad (1)$$

where C_i and C_f are the initial and final TC concentrations (mg L^{-1}), respectively.

The TC uptake (q) was calculated using Equation (2):

$$q = \frac{\left(C_i - C_f\right)V}{m} \quad (2)$$

where q is the amount of TC sorbed (mg g^{-1}), V is the volume of TC solution (L), and m is the mass of CS-HNC (g).

2.5. Sorption Isotherms and Kinetic Studies

Although the Langmuir and Freundlich isotherm models are empirical, they are the most used models to describe sorption equilibrium [26,27]. Equilibrium experiments were conducted at pH 4 with 50 mg of CS-HNC sorbent suspended in 15 mL of TC solutions with initial concentrations ranging from 10 to 100 mg L^{-1} and agitated for 120 min. The resulting equilibrium data were subsequently fitted to the Langmuir, Freundlich, and Temkin isotherm models.

The linearized Langmuir equation was expressed as

$$\frac{C_e}{q_e} = \frac{1}{q_{max}b} + \frac{C_e}{q_{max}} \quad (3)$$

where q_{max} is the maximum monolayer sorption capacity (mg g^{-1}), b is the Langmuir constant (L mg^{-1}), and q_e and C_e are sorption uptake (mg g^{-1}) and concentration (mg L^{-1}) at equilibrium, respectively. A plot of C_e/q_e versus C_e results in a straight line, where the slope equals $1/q_{max}$ and the intercept equals $1/(q_{max}b)$.

The Freundlich adsorption model was applied using the following linearized form:

$$\log q_e = \log K_F + \frac{1}{n}\log C_e \quad (4)$$

where q_e is TC uptake (mg g^{-1}) at equilibrium, C_e is the concentration of TC in solution at equilibrium (mg L^{-1}), K_F is the Freundlich constant, and n is an empirical constant. Plotting log q_e versus log C_e, where the slope equals $1/n$ and the intercept equals log K_F.

The Temkin isotherm model was linearized as

$$q_e = \frac{RT}{b_t}\ln A_t + \frac{RT}{b_t}\ln C_e \quad (5)$$

where R is the universal gas constant (8.314 J mol^{-1} K^{-1}), T is the temperature (K), A_t is the equilibrium binding constant (L g^{-1}), and b_t is related to the sorption heat (J mol^{-1}). A plot of q_e versus lnC_e gives a straight line with slope RT/b_t and intercept (RT/b_t) lnA_t.

Kinetic experiments were carried out using 50 mg of CS-HNC suspended in 15 mL of TC solution at pH 4 and agitated at 150 rpm. Samples were collected at predetermined time intervals (0–60 min), and the amount of adsorbed TC at time t (q_t).

The kinetic behavior of TC sorption onto CS-HNC was evaluated using the pseudo-first-order and pseudo-second-order models proposed by Lagergren and Ho and McKay, respectively. The initial concentrations ranged from 10 to 100 mg L^{-1} and time from 0 to 60 min. The use of multiple initial concentrations enabled assessment of the applicability of the kinetic models over a broad concentration range and evaluation of the influence of the concentration gradient on adsorption behavior.

The linear forms of the Lagergren [28] and Ho models [29] are expressed as

$$\log(q_e - q_t) = \log q_e - \frac{k_1}{2.303}t \quad (6)$$

$$\frac{t}{q_t} = \frac{1}{k_2 q_e^2} + \frac{t}{q_e} \quad (7)$$

where q_e and q_t (mg g^{-1}) are the adsorption capacities at equilibrium and at time t, respectively, and k_1 (min^{-1}) is the pseudo-first-order rate constant and k_2 (g mg^{-1} min^{-1}) is the pseudo-second-order rate constant.

The kinetic parameters were obtained from the slopes and intercepts of the corresponding linear plots. For the PFO model, plots of log($q_e - q_t$) versus t were constructed, whereas

for the PSO model, t/q_t was plotted against t. The quality of the model fit was evaluated using the coefficient of determination (R^2). The experimentally determined equilibrium adsorption capacities ($q_{e,exp}$) were compared with the values calculated from both kinetic models ($q_{e,cal}$).

2.6. Desorption, Regeneration and Stability Studies

Desorption experiments were performed using ethanol, $AlCl_3$ solution, and 0.1 mol L^{-1} NaOH as potential desorbing agents. Following adsorption, the sorbent was separated from the solution and contacted with the corresponding desorption solution under stirring. The desorption efficiency was calculated from the amount of TC released into the solution.

For regeneration studies, adsorption–desorption cycles were repeated five consecutive times using 0.1 mol L^{-1} NaOH as the regeneration agent. After each cycle, the sorbent was washed with deionized water and reused in a subsequent adsorption experiment.

The stability of the material was evaluated by immersing 1 g of CS-HNC in 100 mL of deionized water and, separately, in 100 mL of solution adjusted to pH 2 for 24 h. After filtration, the concentrations of Ag, Co, and Fe in the liquid phase were determined by ICP-MS.

3. Results and Discussion

3.1. Characterization of CS-HNC

3.1.1. FE-SEM, EDS and XRD Imaging

The SEM image shows that the CS-HNC spheres are composed of a network of irregular plate-like and blade-like microstructures with rough surfaces and moderate agglomeration (Figure 1).

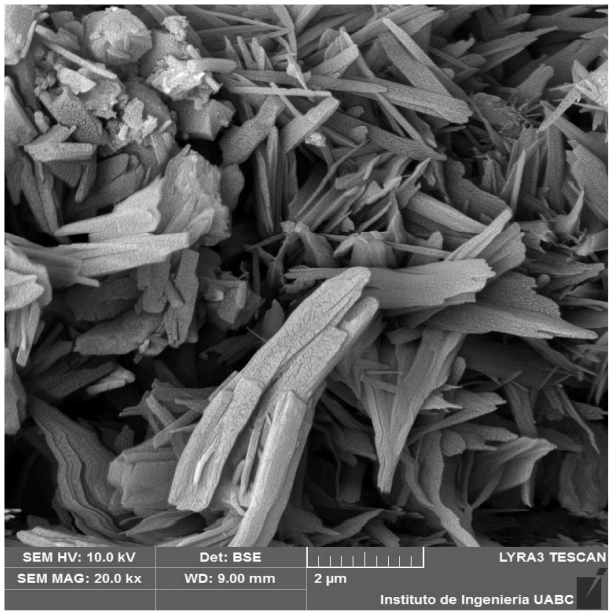


Figure 1. FE-SEM micrograph of the synthesized CS-HNC showing agglomerated plate-like and blade-like microstructures with rough surface morphology.

These observations indicate that the synthesized material possesses a hierarchical microstructure consisting of micro-sized assemblies with nanoscale surface features. Such heterogeneous morphology may be favorable for adsorption processes by providing accessible surface sites for interaction with TC molecules.

The elemental composition of the nanocomposite was analyzed using EDS and the spectrum obtained is shown in Figure A1, and the detected elements are listed in Table 2.

Table 2. Semi-quantitative elemental composition of the CS-HNC nanocomposite determined by EDS analysis (mean ± standard deviation, n = 3).

Element	Series	Wt. % (Mean ± SD)
O	K-series	20.51 ± 1.68
C	K-series	4.25 ± 0.74
Na	K-series	31.86 ± 2.41
Fe	L-series	31.98 ± 7.18
Co	L-series	2.52 ± 0.32
Ag	L-series	10.04 ± 1.40
Ca	K-series	2.57 ± 0.10
Si	K-series	0.86 ± 0.58

n = 3 independent EDS measurements performed at different locations on the sample surface. The elemental compositions are reported as measured by EDS and were not normalized to 100 wt. %. Due to the semi-quantitative nature of EDS, the reported values should be considered approximate elemental compositions.

The presence of C and O is attributed to the chitosan matrix [30], whereas the detection of Fe, Co, and Ag supports the successful incorporation of metal-containing phases into the nanocomposite [21–24]. Similar EDS results confirming the presence of Fe-containing, Co-containing, and magnetic phases in chitosan-based nanocomposites have been reported by Malakootian et al. [21] and Bruckmann et al. [23]. Most likely, Na, Ca, and Si originate from the chitin source material or from the extraction and purification processes used for chitosan production [15]. Residual Na may additionally result from the NaOH solution employed during composite synthesis [17,21].

The XRD pattern of the CS-HNC sorbent (Figure 2B) exhibits a broad diffraction band centered at $2\theta \approx 20^{\circ}$, which is characteristic of the semi-crystalline structure of chitosan [30–33]. In addition, distinct diffraction peaks are observed at $2\theta = 38.24^{\circ}$ and 44.38°, corresponding to the (111) and (200) crystallographic planes of face-centered cubic silver (ICDD/PDF No. 98-006-4997), suggesting the presence of Ag-containing crystalline nanophases within the composite [34]. The broad diffraction peaks suggest the presence of nanosized crystallites dispersed within the polymer matrix [32]. Furthermore, phase-matching analysis indicated the possible presence of hematite (Fe_2O_3) and cobalt hydroxide [$Co(OH)_2$], corresponding to reference patterns 98-009-6077 and 98-005-3994, respectively. The diffraction peaks associated with these phases were weak and partially overlapped with the amorphous chitosan background, suggesting limited crystallinity. This observation is consistent with the nanometric particle size and the partially amorphous nature of the chitosan matrix reported by other researchers [30,35]. Considering the absence of a calcination step but only drying at 50 °C of the CS-HNC, the formation of highly crystalline spinel cobalt ferrite is unlikely. Therefore, the obtained material most likely represents a mixed-phase system composed of Ag-containing nanophases together with possible Fe_2O_3, $Co(OH)_2$, and poorly crystalline cobalt–iron oxide species [21–24,32,33,36–39].

3.1.2. HRTEM and SAED Analysis

HRTEM supported by Fast Fourier transform (FFT) analysis provided molecular-scale insight into the crystalline phases incorporated within the CS-HNC (see Figure 3).

These observations are consistent with the XRD results and support the presence of Ag-, Fe-, and Co-containing crystalline nanophases within the composite (Table 3). The agreement between the experimentally measured lattice spacings and the reference crystallographic values further supports the successful incorporation of inorganic phases into the hybrid nanocomposite structure [21–24,32–34,36,39]. However, the phase assignments

should be considered supportive rather than definitive, as lattice-spacing analysis alone does not provide unambiguous phase identification.

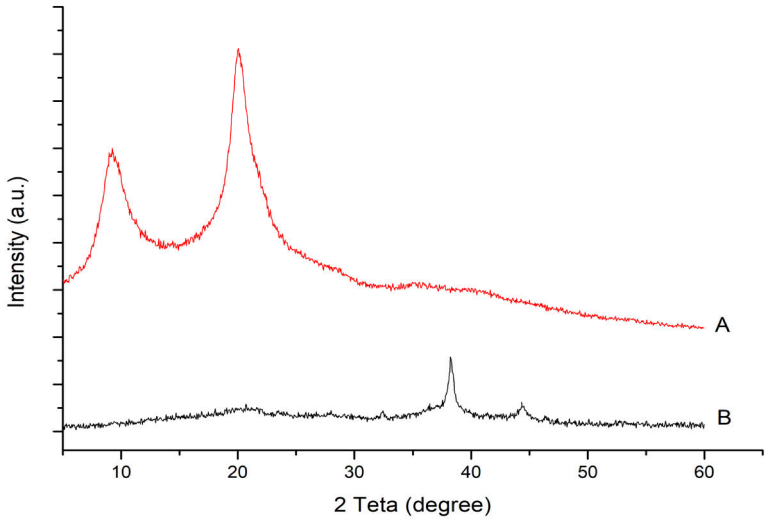


Figure 2. XRD patterns of chitosan (A) and CS-HNC sorbent (B).

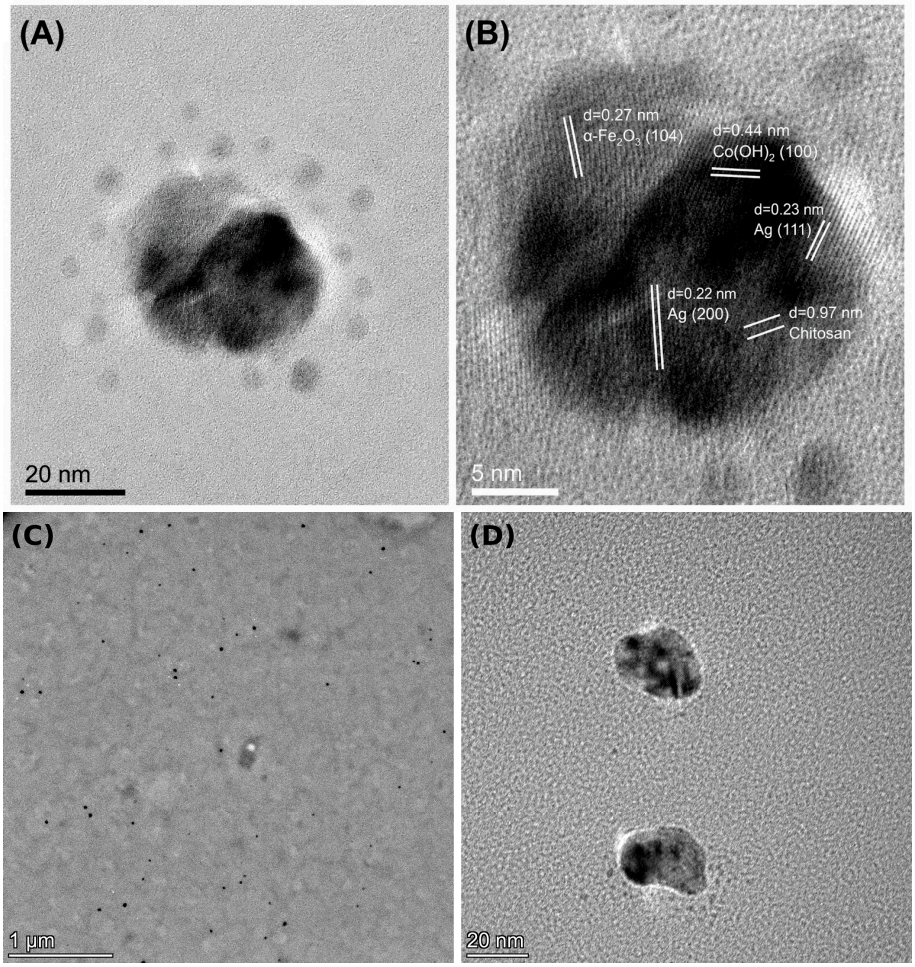


Figure 3. (**A**,**D**) HRTEM image of CS-HNC nanoparticles; (**B**) HRTEM image showing lattice fringes with an interplanar spacing of 0.22, 0.23, 0.27, 0.44, 0.97 nm; (**C**) nanoparticles dispersed in the chitosan matrix.

Table 3. Identification of crystalline phases and corresponding lattice spacings in the CS-HNC nanocomposite.

d-Spacing, nm	Phase	Crystal Structure	Indexed Plane	Ref.
0.22	silver (Ag)	face-centered cubic	(200)	98-006-4997
0.23	silver (Ag)	face-centered cubic	(111)	98-006-4997
0.27	α-hematite (Fe_2O_3)	rhombohedral	(104)	98-009-6077
0.44	$Co(OH)_2$	hexagonal brucite	(100)	98-005-3994
0.97	Chitosan	semi-crystalline polysaccharide	N/A	[35]

The particle size distribution was determined from 100 nanoparticles measured on TEM micrographs (Figure A2). The particle diameters ranged from approximately 10 to 40 nm, with an average diameter of 24 ± 7 nm. Such behavior is commonly observed for polymer-supported metal-containing nanocomposites and is consistent with the heterogeneous morphology of the CS-HNC material [23,32,36].

3.1.3. HRTEM Analysis After TC Sorption

HRTEM examination of the nanocomposite after TC sorption revealed a noticeable increase in particle aggregation compared to the free sorbent (Figure 4).

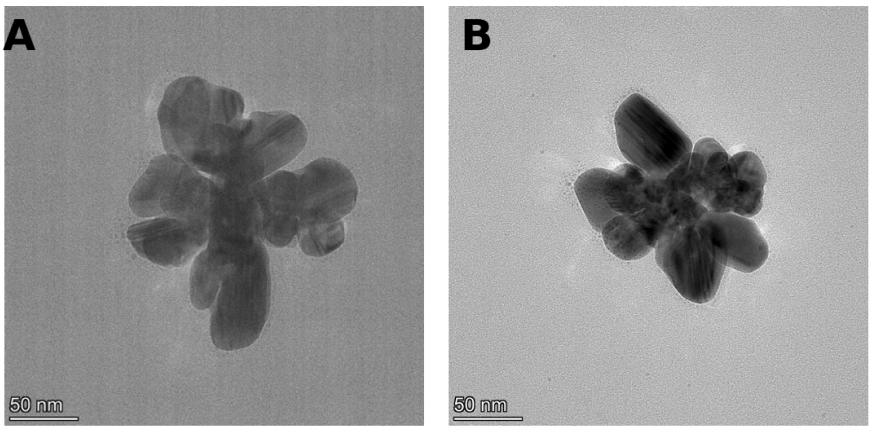


Figure 4. HRTEM images of the CS-HNC nanocomposite after TC sorption. (**A**) Representative nanoparticle aggregate observed within the sample. (**B**) Higher-magnification image showing closely packed nanoparticles.

Prior to sorption, the nanocomposite consisted of discrete nanoparticles with sizes of approximately 10–30 nm. Following TC sorption, larger aggregates (80–150 nm) were observed, although the individual nanoparticles remained distinguishable. The observed increase in aggregate size indicates that morphological changes occurred following TC sorption. However, the mechanism responsible for the observed aggregation was not directly investigated in the present study and therefore no definitive conclusion regarding its origin can be drawn. Similar observations have been reported for other nanocomposite adsorbents following adsorption processes [23,32,36].

3.1.4. Fourier Transform Infrared Spectroscopy (ATR-FTIR)

The FTIR spectra of CS and the synthesized CS-HNC before and after TC sorption are illustrated in Figure 5.

The FTIR spectrum of CS (Figure 5(A)) exhibited a broad absorption band at 3286 cm^{-1} attributed to overlapping O-H and N-H stretching vibrations. The bands observed at 1654 and 1578 cm^{-1} were assigned to Amide I (C=O stretching) and N-H bending vibrations, respectively, while the bands at 1378 and 1030 cm^{-1} corresponded to C-H and C-O vibrations

characteristic of the chitosan backbone. These assignments are consistent with previous reports [30,35]. The bands at 2878 and 894 cm^{-1} further confirmed the preservation of the characteristic chitosan structure. Compared with CS, the FTIR spectrum of CS-HNC (Figure 5(B)) exhibited several modifications, including a shift of the broad hydroxyl band to 3465 cm^{-1} and the appearance of a band at 3043 cm^{-1}, indicating changes in the functional groups following incorporation of the inorganic phases [32,39]. In addition, a band at 564 cm^{-1} was observed, which is consistent with metal–oxygen vibrations reported for iron- and cobalt-containing species [32,33,36]. Additional bands at 1450 and 846 cm^{-1} may be associated with coordinated carbonate species. After TC sorption (Figure 5(C)), further spectral changes were observed. A band appeared at 2886 cm^{-1}, while the intensity of the band at 1643 cm^{-1} increased. Furthermore, slight shifts of the C-O stretching band to 1020 cm^{-1} and of the carbonate-related band to 1373 cm^{-1} were detected. These spectral modifications suggest interactions between TC molecules and functional groups present on the CS-HNC surface [23,36].

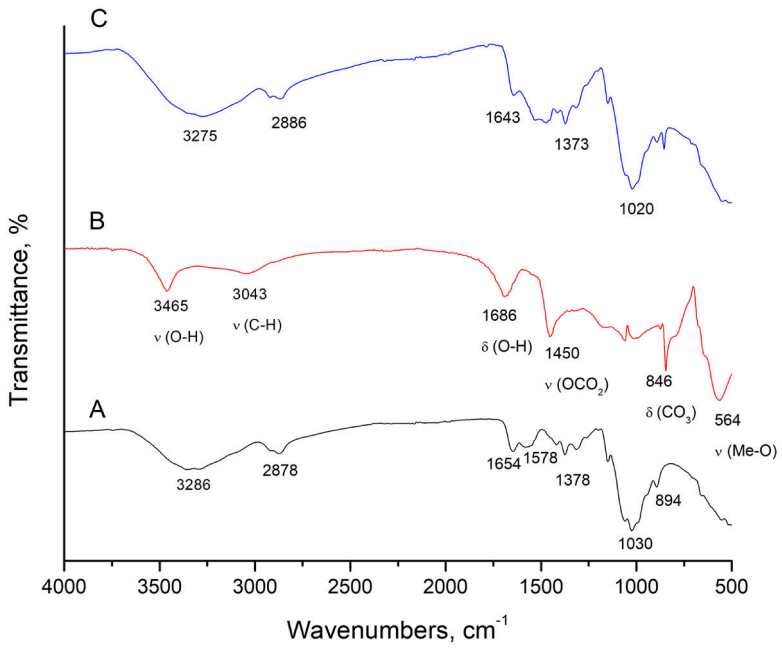


Figure 5. FTIR spectra of chitosan (A), CS-HNC (B), and CS-HNC after TC sorption (C).

3.1.5. Point of Zero Charge (pHPZC)

The pH_{PZC} value of the CS-HNC sorbent was determined to be approximately 9.6–9.8 (Figure 6). At pH values below pH_{PZC}, the sorbent surface is positively charged, while above pH_{PZC} it becomes negatively charged. The adsorption behavior of TC may be influenced by changes in surface charge together with other interactions between TC molecules and the functional groups present on the adsorbent surface. The high pH_{PZC} of CS-HNC suggests that the sorbent surface remains positively charged throughout most of the investigated pH range.

3.2. Effect of Process Parameters on TC Removal

In a preliminary study, the CS-HNC was evaluated regarding its potential to remove TC from aqueous solutions. Under these experimental conditions (sorbent concentration 0.1 g/100 mL, initial TC concentration of 50 mg L^{-1}, pH 4.0, contact time of 2 h), the nanocomposite removed 65.9% of TC. Based on these results, further optimization of sorption conditions and sorption studies were carried out.

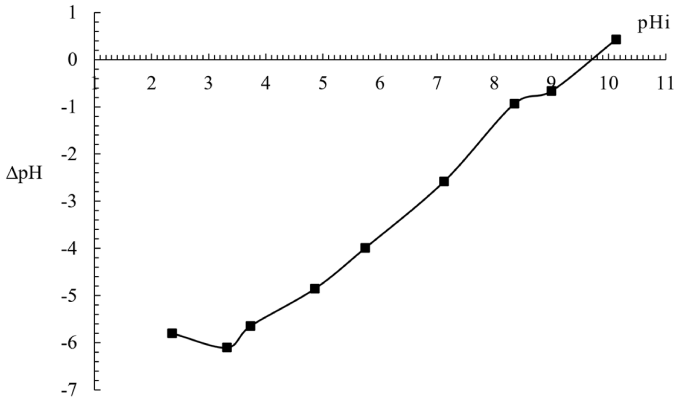


Figure 6. Plot of ΔpH versus initial pH (pHi) for determination of the point of zero charge (pH_{PZC}) of CS-HNC sorbent.

3.2.1. Influence of Initial pH of Solution on TC Sorption

The pH of the solution does not affect only the surface charge of the sorbent but also influences the charge and chemical speciation of the TC molecule.

The influence of the initial solution pH on TC sorption was investigated in the pH range from 3 to 9 (Figure 7). The results show that pH has a relatively minor effect on TC removal, with sorption efficiencies ranging from 94.6% to 97.4%, suggesting affinity of the nanocomposite toward TC over a wide pH range.

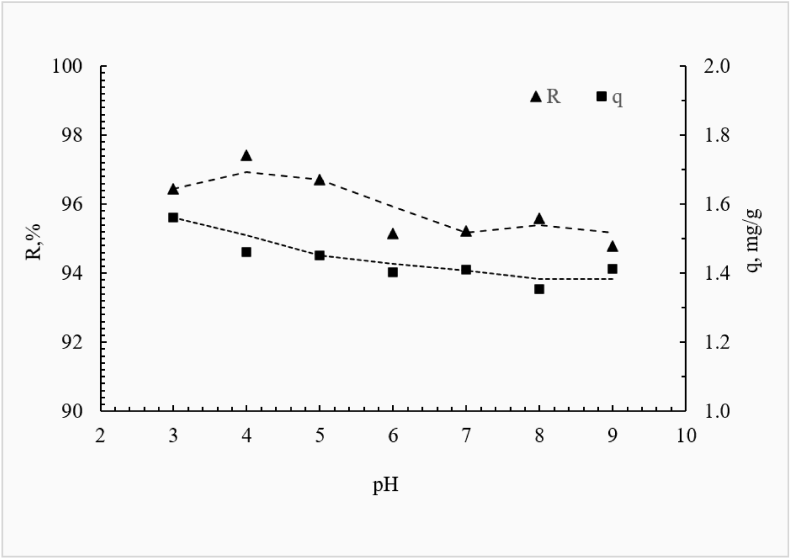


Figure 7. Effect of pH on TC removal (R, %) and sorption capacity (q, mg g^{-1}). (Ci(TC) = 10 mg L^{-1}; t = 2 h; m(CS-HNC) = 0.1 g; V = 15 mL; stirring speed of 150 rpm).

At pH values below 3.3, TC predominantly exists in its cationic form (TCH_3^+) due to protonation of the dimethylamino group [1,2,4]. Despite the electrostatic repulsion expected between the positively charged sorbent surface and the cationic TC species, the removal efficiency remained high, suggesting that electrostatic interactions alone cannot fully explain the observed adsorption behavior.

The highest experimental TC removal was observed at pH 4. However, the removal efficiencies obtained within the investigated pH range differed by less than 3 percentage points (94.6–97.4%), indicating only a weak dependence of adsorption performance on pH. Therefore, pH 4 should be regarded as the condition at which the highest experimental removal efficiency was observed rather than a pronounced optimum. In the pH range

3.3–7.7, TC mainly exists in its zwitterionic form ($TCH_2\pm$), resulting from deprotonation of the tricarbonyl/phenolic diketone system [1,2,4]. Enhanced sorption under mildly acidic conditions was also reported by Nasiri et al. [36] for $CuCoFe_2O_4$@chitosan nanocomposites used for TC removal.

At pH values above 7.7, further deprotonation occurs and TC progressively transforms into its anionic form (TCH^- and TC^{2-}) [1,2,4]. Since the pH_{PZC} of the CS-HNC sorbent is approximately 9.6–9.8, the sorbent surface remains positively charged throughout the investigated pH range, favoring electrostatic attraction toward negatively charged TC species. Similar observations were reported by Zhang et al. [40], who found only minor differences in the sorption of TC, oxytetracycline, and chlortetracycline on amino-Fe(III)-functionalized SBA-15 at different pH values.

The relatively high TC removal efficiency over the entire pH range investigated (94.6–97.4%) demonstrates that sorption is not strongly pH-dependent. This behavior suggests that electrostatic interactions alone are insufficient to explain the observed adsorption behavior and that additional interactions between TC molecules and functional groups present on the CS-HNC sorbent surface may also contribute to adsorption [20,36]. The limited variation in removal efficiency and sorption capacity indicates that the CS-HNC sorbent can effectively remove TC under both acidic and alkaline conditions, which may be advantageous for practical wastewater treatment applications. Similar behavior has been reported for other chitosan-based composite adsorbents used for TC removal [41,42].

3.2.2. Effect of CS-HNC Dosage on TC Removal Efficiency

The influence of the amount of CS-HNC sorbent on TC removal was studied in the range of 25–150 mg (Figure 8). A TC removal efficiency of 97.8% was achieved using 50 mg of CS-HNC, while no pronounced increase was observed when the sorbent dosage was further increased to 100 or 150 mg.

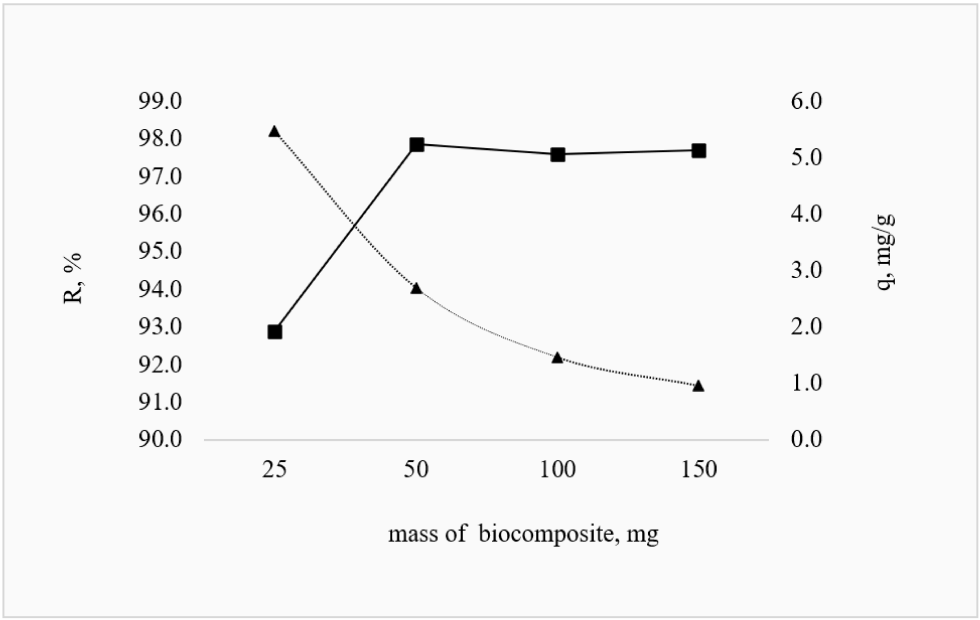


Figure 8. Effect of CS-HNC dosage on TC sorption. The square symbols (■) represent the removal efficiency (*R*, %) plotted on the left y-axis, while the triangle symbols (▲) represent the equilibrium adsorption capacity (q, mg g^{-1}) plotted on the right y-axis. Experimental conditions: pH 4; C_i(TC) = 10 mg/L; V = 15 mL; 150 rpm.

TC sorption depends on the availability of active sites on the surface of the CS-HNC sorbent. Owing to the presence of multiple functional groups in the TC molecule, including

hydroxyl, amide, and carbonyl groups [1–4], increasing the sorbent dosage initially enhanced TC removal due to the greater number of available sorption sites. At higher dosages, particle aggregation may occur, reducing the effective surface area and accessibility of adsorption sites, while a fraction of the available sites may remain unused. Similar behavior has been reported for other chitosan-based adsorbents used for TC removal [23,36,42]. Therefore, a dosage of 50 mg CS-HNC was selected for subsequent experiments.

3.2.3. Effect of Contact Time and Initial TC Concentration

To investigate the effect of contact time (2.5–120 min) on TC sorption, solutions with different initial concentrations were prepared and mixed with 50 mg of sorbent. After a fixed interval of time, the sorption process was stopped, and the TC concentration was determined. The obtained results are shown in Figure 9.

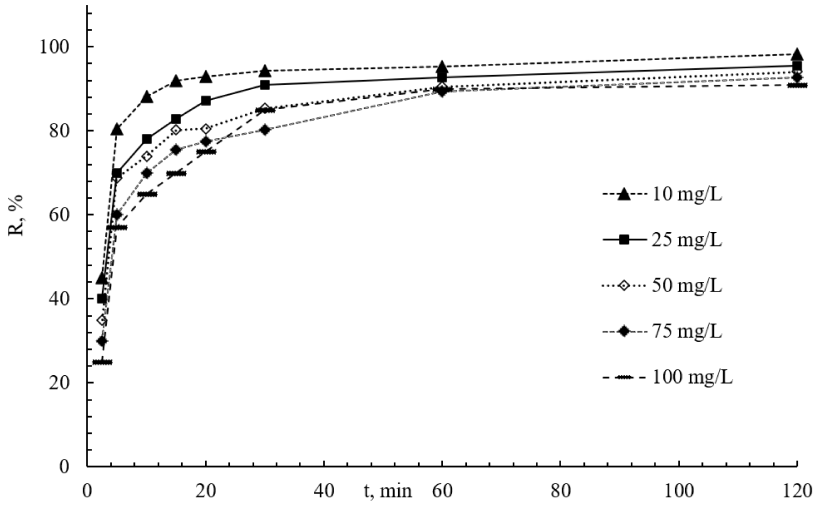


Figure 9. Effect of contact time on TC removal by CS-HNC at different initial TC concentrations (m = 50 mg, V = 15 mL, pH = 4).

The removal efficiency decreased from 98.3% to 91.0% as the initial TC concentration increased from 10 to 100 mg L^{-1}, respectively. The highest removal efficiency was obtained at the lowest TC concentration, owing to the greater availability of active sorption sites on the sorbent surface. As the initial concentration increased, the available sorption sites gradually became saturated, resulting in a decrease in removal efficiency. This phenomenon is well documented in adsorption studies and reflects the finite adsorption capacity of the sorbent and the increasing adsorbate-to-site ratio at higher initial concentrations [23,36,42].

Rapid sorption occurred during the first 5 min, with 80.4% of TC removed, indicating a high affinity of the CS-HNC sorbent toward TC. The removal efficiency increased to 94.3% after 30 min at an initial TC concentration of 10 mg L^{-1}. After 30 min, only minor changes in TC removal were observed, suggesting that the adsorption system had approached equilibrium. The removal efficiency reached 98.3% after 120 min. The process approached equilibrium within approximately 60 min. Similar behavior has been reported for other chitosan-based adsorbents used for TC removal. Nasiri et al. [36] investigated the removal of TC onto $CuCoFe_2O_4$@chitosan nanoparticles and achieved a maximum removal efficiency of 93.07% under optimized conditions (TC concentration 5 mg L^{-1}, pH 3.5, adsorbent dosage 0.4 g L^{-1}, temperature 25 °C, and contact time 30 min). Likewise, Bruckmann et al. [23] reported highly efficient TC sorption using a magnetic chitosan-based adsorbent, suggesting the strong affinity of chitosan-containing nanocomposites toward TC. Comparable effects have also been described for metal-modified chitosan composites by Turan et al. [42].

3.2.4. Influence of Ionic Strength of the Solution

The influence of ionic strength was investigated using 0.01, 0.1, and 0.5 M NaCl solutions (Ci = 75 mg L^{-1}, V = 15 mL, m(CS-HNC) = 50 mg, pH 4, t = 60 min). The corresponding removal efficiencies were 89.0%, 90.5%, and 91.3%, respectively, indicating that increasing ionic strength had only a minor effect on TC adsorption. Similar results were observed by other researchers [36,40,42].

3.3. Sorption Isotherms and Kinetic Studies

The equilibrium adsorption data were analyzed using Langmuir, Freundlich, and Temkin isotherm models. The corresponding linearized plots are presented in Figure 10.

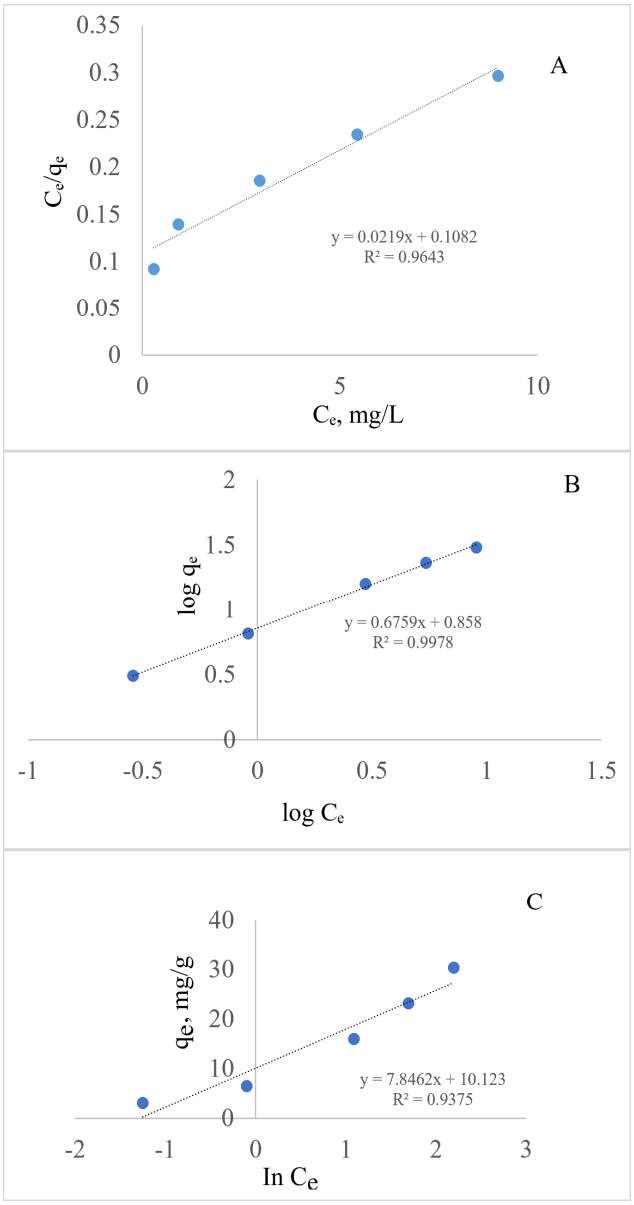


Figure 10. Linearized plots for Langmuir (**A**), Freundlich (**B**) and Temkin (**C**) isotherm models (pH 4, m = 50 mg, V = 15 mL, t = 120 min, initial TC concentrations = 10–100 mg L^{-1}).

The isotherm constants calculated from the Langmuir, Freundlich, and Temkin models, together with the correlation coefficients, are presented in Table 4.

Table 4. Isotherm parameters for TC sorption onto CS-HNC obtained from Langmuir, Freundlich, and Temkin models.

Langmuir Model			Freundlich Model			Temkin		
q_{max}, mg g^{-1}	b, L mg^{-1}	R^2	K_F, (mg g^{-1})(mg L^{-1})$^{1/n}$	n	R^2	b_t, J mol^{-1}	A_t L g^{-1}	R^2
45.7	0.202	0.964	7.21	1.48	0.998	316	3.63	0.937

The adsorption equilibrium data were satisfactorily described by both the Langmuir and Freundlich models. The Langmuir model yielded a maximum adsorption capacity (q_{max}) of 45.7 mg g^{-1}, while the Freundlich model exhibited the highest correlation coefficient (R^2 = 0.998), indicating a better fit to the experimental data. The Freundlich constant n was 1.48, corresponding to a value of 1/n = 0.68. Since 1/n lies between 0 and 1, TC adsorption onto CS-HNC can be considered favorable under the investigated conditions. The lower correlation coefficient obtained for the Temkin model (R^2 = 0.937) suggests that this model provides a less accurate description of the adsorption equilibrium.

The adsorption kinetics of TC sorption onto CS-HNC were analyzed using the pseudo-first-order (PFO) and pseudo-second-order (PSO) kinetic models. The PFO and PSO plots were constructed using the data obtained during the initial adsorption stage, where the most pronounced changes in adsorption capacity occurred. The corresponding linearized plots are presented in Figures 11 and 12.

The calculated rate constants, equilibrium sorption capacities, and correlation coefficients are presented in Table 5.

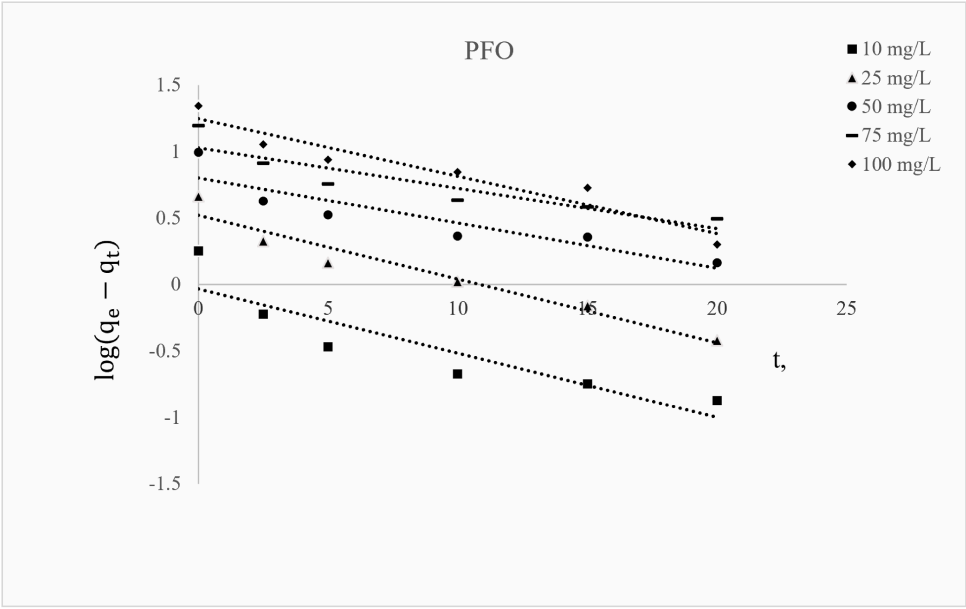


Figure 11. PFO kinetic model plots of TC sorption onto CS-HNC at different initial concentrations (c(TC) = 10–100 mg L^{-1}; m(CS-HNC) = 0.05 g, V = 15 mL, pH = 4).

The experimentally determined adsorption capacities ($q_{e,exp}$) reported in Table 5 correspond to the adsorption capacities obtained at 60 min, which was the final time point included in the kinetic-model fitting procedure. The experimentally determined adsorption capacities ($q_{e,exp}$) increased from 3.22 to 25.67 mg g^{-1} as the initial TC concentration increased from 10 to 100 mg L^{-1}. For all investigated concentrations, the PSO model showed substantially higher correlation coefficients (R^2 = 0.996–0.984) than the PFO model (R^2 = 0.941–0.809). Furthermore, the equilibrium adsorption capacities predicted by the PSO model were in closer agreement with the experimentally determined values than those

obtained from the PFO model. Similar findings have been reported for TC adsorption onto chitosan-based and magnetic chitosan composites, where the PSO model consistently provided a better description of the adsorption kinetics than the PFO model [23,36,42]. These results indicate that the PSO model provides a more accurate description of TC adsorption onto CS-HNC over the investigated concentration range.

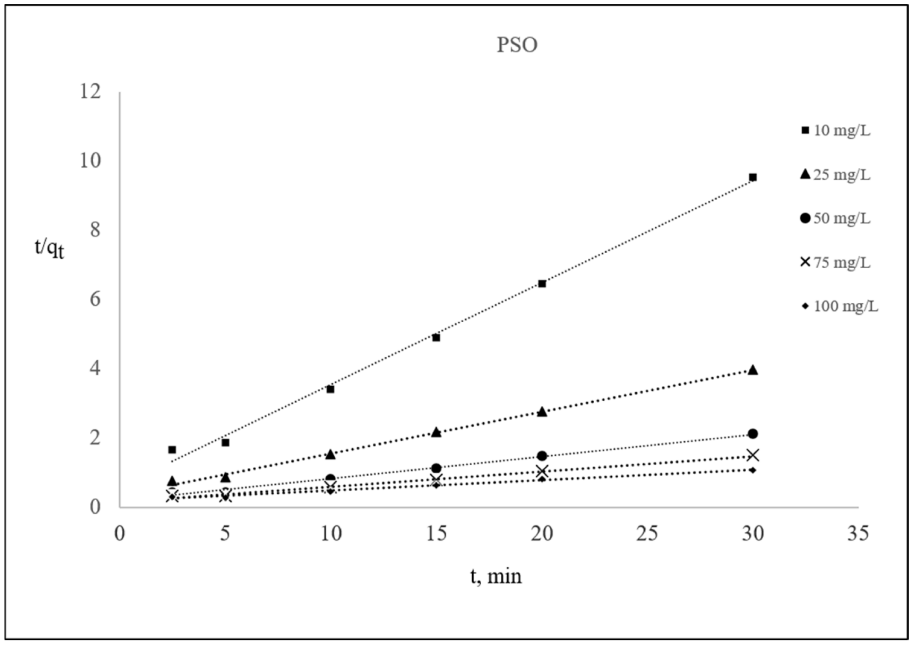


Figure 12. Linearized PSO kinetic model for TC sorption onto CS-HNC at initial concentrations of 10, 25, 50, 75, and 100 mg L^{-1} (m(CS-HNC) = 0.05 g, V = 15 mL, pH = 4).

Table 5. Kinetic parameters of TC sorption onto CS-HNC determined using PFO and PSO models.

		PFO Kinetic Model			PSO Kinetic Model		
C_i, mg L^{-1}	$q_{e,exp}$ mg g-1	$q_{e\ (cal)}$, mg g^{-1}	k_1, min^{-1}	R^2	$q_{e(cal)}$, mg g^{-1}	k_2, g mg^{-1} min^{-1}	R^2
10	3.22	1.08	11.1×10^{-2}	0.809	3.39	148×10^{-3}	0.996
25	7.49	1.13	10.9×10^{-2}	0.941	8.34	40.3×10^{-3}	0.997
50	13.67	6.31	7.80×10^{-2}	0.825	15.6	21.7×10^{-3}	0.994
75	20.58	10.7	7.00×10^{-2}	0.826	22.8	12.4×10^{-3}	0.992
100	25.67	17.7	9.79×10^{-2}	0.919	33.4	5.06×10^{-3}	0.984

3.4. Sorption–Desorption Studies of the CS-HNC Sorbent

Desorption and stability studies were performed to evaluate the regeneration potential and structural robustness of the CS-HNC sorbent. Ethanol, $AlCl_3$, and 0.1 mol L^{-1} NaOH were investigated as desorbing agents. Ethanol and $AlCl_3$ exhibited limited desorption efficiency and were unable to recover a substantial fraction of the adsorbed TC. In contrast, NaOH was found to be the most effective regeneration agent (approximately 95% of TC was desorbed) and was therefore selected for subsequent reusability experiments. Similar observations have been reported for TC-loaded chitosan-based adsorbents, where alkaline solutions facilitate desorption more effectively than neutral solvents or salt solutions [23,36,42].

The reusability of the CS-HNC sorbent was evaluated through five consecutive adsorption–desorption cycles using 0.1 mol L^{-1} NaOH as the regeneration agent. A gradual decrease in adsorption performance was observed with increasing cycle number. After five

cycles, the adsorption efficiency decreased by approximately 30% compared with the initial cycle. Similar decreases in adsorption performance after repeated regeneration cycles have been reported for other chitosan-based and magnetic nanocomposite adsorbents and are commonly attributed to incomplete desorption of adsorbed molecules, blockage of active sites, surface modification, or structural changes occurring during repeated use [23,36]. However, the exact contribution of the individual deactivation mechanisms was not investigated in the present study. Nevertheless, the material retained approximately 70% of its initial adsorption efficiency after five adsorption–desorption cycles, demonstrating satisfactory reusability. This performance is comparable to that reported for other chitosan-based magnetic adsorbents used for TC removal [23,36].

The chemical stability of CS-HNC was further assessed by leaching experiments. One gram of the nanocomposite was immersed in 100 mL of deionized water for 24 h, after which the solution was analyzed by inductively coupled plasma mass spectrometry (iCAP Q ICP-MS, Thermo Fisher Scientific, Waltham, MA, USA). In addition, the sorbent was exposed to an aqueous solution adjusted to pH 2 for 24 h to evaluate its stability under acidic conditions. ICP-MS analysis revealed no detectable leaching of Fe, Co, or Ag from the material under the investigated conditions. No detectable difference in metal concentration was observed between the treated samples and the corresponding blank solutions. These findings indicate negligible metal release and suggest good structural stability of the CS-HNC nanocomposite, even under strongly acidic conditions.

3.5. Limitations and Future Work

Although the CS-HNC nanocomposite demonstrated high TC removal efficiency under laboratory conditions, several limitations should be acknowledged. The adsorption experiments were conducted using controlled batch systems and model aqueous solutions containing TC as the sole target contaminant. Therefore, the performance of the material in real wastewater matrices containing competing ions, dissolved organic matter, and other contaminants remains to be evaluated. In addition, although the sorbent retained a substantial fraction of its initial adsorption capacity after five adsorption–desorption cycles and no detectable Ag, Fe, or Co leaching was observed under the investigated stability-testing conditions, further studies involving longer exposure periods, extended regeneration cycles, and continuous-flow operation are required to fully assess the long-term stability and practical applicability of the material. Consequently, the present results should be considered a proof-of-concept demonstration of the adsorption potential of the developed nanocomposite rather than a comprehensive assessment of its large-scale performance.

To place the developed material into the context of currently reported TC adsorbents, a comparison of preparation complexity and reusability is presented in Table 6.

As shown in Table 6, many reported chitosan-based and magnetic adsorbents involve multistep synthesis procedures and the preparation of metal-containing nanoparticles prior to incorporation into the polymer matrix [13,23,36]. In contrast, the CS-HNC nanocomposite was synthesized by a one-step coprecipitation method under mild conditions without high-temperature calcination while maintaining high TC removal efficiency, satisfactory reusability, and good chemical stability.

While biological treatment, ozonation, and activated-carbon adsorption are already applied in full-scale water and wastewater treatment, advanced nanocomposite adsorbents remain largely at the laboratory stage. A comparison table of currently applied treatment methods and the proposed adsorbent is presented in Table 7.

Table 6. Comparison of selected TC adsorbents reported in the literature and the developed CS-HNC nanocomposite.

Adsorbent Type	Preparation Procedure	Calcination Required	Reusability Reported	Remarks	Ref.
Mineral adsorbents	Direct use or simple modification of mineral materials	No	Limited information	Simple preparation, generally lower adsorption capacity than engineered composites	[10]
Silica-based adsorbents	Surface functionalization of silica materials	Usually no	Reported	Efficient TC removal but requires surface modification procedures	[11]
Fe_3O_4-chitosan/ZIF-8 beads	Multistep synthesis involving magnetic and MOF components	Yes	5 cycles (>60% capacity retained)	High TC removal efficiency but more complex synthesis route	[13]
$CuCoFe_2O_4$@chitosan nanocomposite	Synthesis of magnetic nanoparticles followed by incorporation into chitosan	Yes	Reported (up to 5 cycles)	High adsorption performance but nanoparticle preparation is required	[36]
Magnetic chitosan adsorbent	Multistep preparation	Usually required for magnetic phase synthesis	Reported (several adsorption/desorption cycles)	Efficient adsorption and magnetic separation capability	[23]
CS-HNC (this study)	One-step coprecipitation in aqueous meium	No	Yes 5 cycles (~70% capacity retained)	One-step coprecipitation, no calcination, 5 regeneration cycles, no detectable Ag, Co, or Fe leaching.	This study

Table 7. Comparison of currently applied TC-removal technologies and the developed CS-HNC adsorbent.

Method	Main Advantage	Main Limitation	Relative Energy Demand	Expected Carbon Footprint *	Ref.
Biological treatment	Widely implemented in wastewater treatment plants	Incomplete removal of antibiotics may occur	Low to moderate	Moderate	[7]
Ozonation	Rapid degradation of TC	Requires ozone generation and energy input	High	High	[5]
Photo-Fenton oxidation (AOP)	High degradation efficiency	Requires oxidants and pH control	High	High	[6]
Adsorption	Simple operation and possibility for sorbent regeneration	Requires adsorbent regeneration or replacement	Low to moderate	Low to moderate	[10–16]
CS-HNC (this study)	Mild synthesis conditions (50 °C), no calcination step, reusable sorbent (5 cycles)	Evaluated only under laboratory batch conditions	Low	Potentially low	This study

* Qualitative assessment based on process requirements and energy demand reported in the literature. A detailed life-cycle assessment and carbon-footprint analysis were beyond the scope of the present study.

4. Conclusions

A novel CS-HNC nanocomposite was successfully synthesized and evaluated for the removal of TC from aqueous solutions. The material exhibited good sorption performance, achieving 94.3% TC removal within 30 min and 98.4% after 120 min for an initial TC concentration of 10 mg L^{-1}. The sorption equilibrium data were better described by the Freundlich isotherm model (R^2 = 0.998) than by the Langmuir and Temkin models. The Freundlich constant (n = 1.48) indicates favorable sorption of TC. The maximum sorption

capacity estimated by the Langmuir model was 45.7 mg g^{-1}, demonstrating a moderate-to-high affinity of the developed sorbent toward TC.

From a practical perspective, the high removal efficiency achieved at relatively low TC concentrations, together with the limited influence of pH and ionic strength, suggests that the CS-HNC nanocomposite shows potential for the treatment of waters containing low concentrations of pharmaceutical contaminants. These characteristics may be advantageous for future wastewater treatment applications.

Furthermore, ICP-MS analysis revealed no detectable leaching of Ag, Co, or Fe after exposure to deionized water and acidic solution (pH 2), indicating good stability of the nanocomposite under the investigated conditions.

Although the present study was conducted under laboratory batch conditions using synthetic solutions, the obtained results demonstrate the potential of the developed CS-HNC nanocomposite for TC removal and justify further studies under real wastewater and continuous-flow conditions.

Author Contributions: Conceptualization, G.K.; Methodology, G.K.; Investigation, G.K., M.S., N.Z., G.A., Z.V. and V.G.; Formal analysis, G.K.; Data curation, G.K.; Writing—original draft preparation, G.K.; Writing—review and editing, G.K., Z.V., V.G. and M.S. All authors have read and agreed to the published version of the manuscript.

Funding: This research received no external funding.

Institutional Review Board Statement: Not applicable.

Informed Consent Statement: Not applicable.

Data Availability Statement: The original contributions presented in this study are included in the article. Further inquiries can be directed to the corresponding author.

Conflicts of Interest: The authors declare no conflicts of interest.

Abbreviations

The following abbreviations are used in this manuscript:

TC	Tetracycline
CS-HNC	Chitosan-based hybrid nanocomposite
EDS	Energy-Dispersive X-ray Spectroscopy
FE-SEM	Field-Emission Scanning Electron Microscopy
FTIR	Fourier Transform Infrared Spectroscopy
HRTEM	High-Resolution Transmission Electron Microscopy
SAED	Selected Area Electron Diffraction

Appendix A

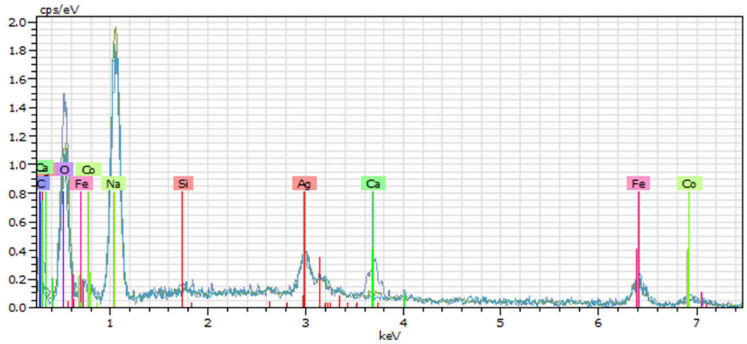


Figure A1. EDS spectrum of the synthesized CS-HNC sorbent.

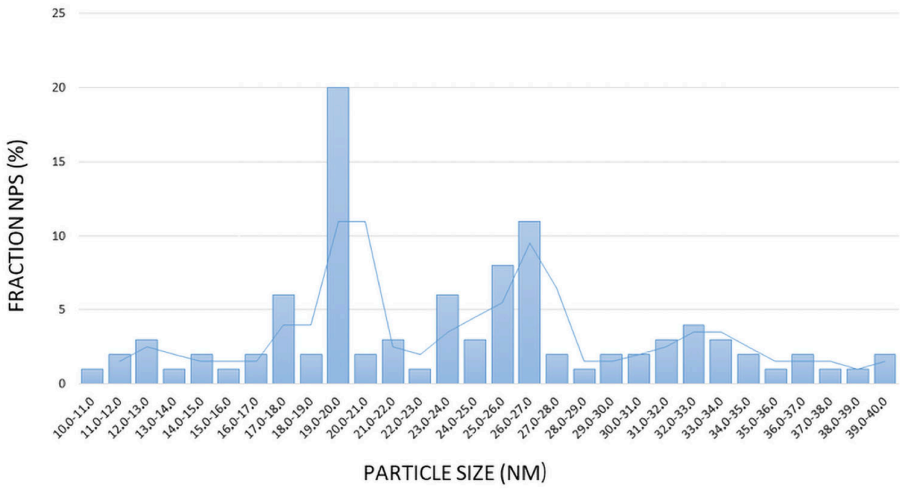


Figure A2. Particle size distribution of CS-HNC nanoparticles is determined from measurements of 100 particles. The particle diameters ranged from approximately 10 to 40 nm, with an average particle size of 24 ± 7 nm. The line is included to visualize the overall distribution trend.

References

1. Chopra, I.; Roberts, M. Tetracycline antibiotics: Mode of action, applications, molecular biology, and epidemiology of bacterial resistance. *Microbiol. Mol. Biol. Rev.* **2001**, *65*, 232–260. [CrossRef]
2. Ahmad, F.; Zhu, D.; Sun, J. Environmental fate of tetracycline antibiotics: Degradation pathway mechanisms, challenges, and perspectives. *Environ. Sci. Eur.* **2021**, *33*, 64. Correction in *Environ. Sci. Eur.* **2021**, *33*, 71.. [CrossRef]
3. Scaria, J.; Anupama, K.V.; Nidheesh, P.V. Tetracyclines in the environment: An overview on occurrence, fate, toxicity, detection, removal methods, and sludge management. *Sci. Total Environ.* **2021**, *771*, 145291. [CrossRef]
4. Nelson, M.L.; Theuretzbacher, U.; Dale, G.E. Tetracycline Derivatives and Tetracycline Mimetics: Biology, Chemistry, and Human Use. *J. Med. Chem.* **2024**, *67*, 7395–7427. [CrossRef]
5. Wang, C.; Lin, C.-Y.; Liao, G.-Y. Feasibility study of tetracycline removal by ozonation equipped with an ultrafine-bubble compressor. *Water* **2021**, *13*, 1058. [CrossRef]
6. Han, C.-H.; Park, H.-D.; Kim, S.-B.; Yargeau, V.; Choi, J.-W.; Lee, S.-H.; Park, J.-A. Oxidation of tetracycline and oxytetracycline by the photo-Fenton process: Their transformation products and toxicity assessment. *Water Res.* **2020**, *172*, 115514. [CrossRef]
7. Wu, X.; Gu, Y.; Wu, X.; Zhou, X.; Zhou, H.; Amanze, C.; Shen, L.; Zeng, W. Construction of a tetracycline-degrading bacterial consortium and its application in laboratory-scale soil remediation. *Microorganisms* **2020**, *8*, 292. [CrossRef]
8. Sousa, J.F.M.; Murtinho, D.; Valente, A.J.M.; Marques, J.M.C. The Role of Chitosan-Based Materials in Interactions with Antibiotics: An Overview of In Vitro and In Silico Studies. *Int. J. Mol. Sci.* **2025**, *26*, 11070. [CrossRef]
9. Ersan, M.; Dogan, H. Development of new adsorbents via microwave treatment magnetic PET synthesis from waste PET and investigation of tetracycline removal. *Colloid Interface Sci. Commun.* **2021**, *42*, 100416. [CrossRef]
10. Cuevas, J.; Dirocie, N.; Yunta, F.; Delgado, C.G.; Santamaría, D.E.G.; Ruiz, A.I.; Fernández, R.; Eymar, E. Evaluation of the sorption potential of mineral materials using tetracycline as a model pollutant. *Minerals* **2019**, *9*, 453. [CrossRef]
11. Althumayri, K.; Guesmi, A.; Abd El-Fattah, W.; Houas, A.; Ben Hamadi, N.; Shahat, A. Enhanced adsorption and evaluation of tetracycline removal in an aquatic system by modified silica nanotubes. *ACS Omega* **2023**, *8*, 6762–6777. [CrossRef]
12. Mohammed, A.A.; Al-Musawi, T.J.; Kareem, S.L.; Zarrabi, M.; Al-Ma'abreh, A.M. Simultaneous adsorption of tetracycline, amoxicillin, and ciprofloxacin by pistachio shell powder coated with zinc oxide nanoparticles. *Arab. J. Chem.* **2020**, *13*, 4629–4643. [CrossRef]
13. Amanizadegan, M.; Vafajoo, L.; Soleimani, M. Magnetically recoverable Fe_3O_4-chitosan/ZIF-8 beads for tetracycline removal from aqueous solution. *Sci. Rep.* **2026**, *16*, 24557. [CrossRef]
14. Nasiri, A.; Golestani, N.; Rajabi, S.; Hashemi, M. Facile and green synthesis of recyclable, environmentally friendly, chemically stable magnetic nanohybrid adsorbent for tetracycline adsorption. *Heliyon* **2024**, *10*, e24179. [CrossRef]
15. Hasan, M.M.; Habib, L.; Anwaruzzaman, M.; Kamruzzaman, M.; Khan, M.N.; Rahman, M.M. Processing techniques of chitosan-based interpenetrating polymer networks, gels, blends, composites and nanocomposites. In *Handbook of Chitin and Chitosan*; Gopi, S., Thomas, S., Pius, A., Eds.; Elsevier: Amsterdam, The Netherlands, 2020; pp. 61–93. [CrossRef]

16. Pishevar, A.; Khanchoupan, M.; Afradi, A.; Kazemian, F.; Behbudi, G. Recent developments in chitosan-based adsorbents for tetracycline removal: A mini-review. *Synth. Sinter.* **2025**, *5*, 100038. [CrossRef]
17. Gupta, A.; Chauhan, V.S.; Sankararamakrishnan, N. Preparation and evaluation of iron–chitosan composites for removal of As(III) and As(V) from arsenic-contaminated groundwater. *Water Res.* **2009**, *43*, 3862–3870. [CrossRef]
18. Lapo, B.; Demey, H.; Carchi, T.; Sastre, A.M. Antimony removal from water by a chitosan–iron(III) [ChiFer(III)] nanocomposite. *Polymers* **2019**, *11*, 351. [CrossRef]
19. Carlotti, A.; Cesaretti, A.; Elisei, F. Complexes of tetracyclines with divalent metal cations investigated by stationary and femtosecond-pulsed techniques. *Phys. Chem. Chem. Phys.* **2012**, *14*, 823–834. [CrossRef]
20. Gu, C.; Karthikeyan, K.G. Interaction of tetracycline with aluminum and iron hydrous oxides. *Environ. Sci. Technol.* **2005**, *39*, 2660–2667. [CrossRef]
21. Malakootian, M.; Nasiri, A.; Mahdizadeh, H. Preparation of $CoFe_2O_4$/activated carbon@chitosan as a new magnetic nanonanocomposite for adsorption of ciprofloxacin in aqueous solutions. *Water Sci. Technol.* **2018**, *78*, 2158–2170. [CrossRef]
22. Yang, C.-H.; Wang, C.-Y.; Huang, K.-S.; Yeh, C.-S.; Wang, A.H.-J.; Wang, W.-T.; Lin, M.-Y. Facile synthesis of radial-like macroporous superparamagnetic chitosan spheres with in situ co-precipitation and gelation of ferro-gels. *PLoS ONE* **2012**, *7*, e49329. [CrossRef]
23. Bruckmann, F.d.S.; Schnorr, C.E.; Salles, T.d.R.; Nunes, F.B.; Baumann, L.; Müller, E.I.; Silva, L.F.O.; Dotto, G.L.; Rhoden, C.R.B. Highly efficient adsorption of tetracycline using chitosan-based magnetic adsorbent. *Polymers* **2022**, *14*, 4854. [CrossRef]
24. Sipos, P.; Berkesi, O.; Tombácz, E.; Pierre, T.G.S.; Webb, J. Formation of spherical iron(III) oxyhydroxide nanoparticles sterically stabilized by chitosan in aqueous solutions. *J. Inorg. Biochem.* **2003**, *95*, 55–63. [CrossRef]
25. Fiol, N.; Villaescusa, I. Determination of sorbent point zero charge: Usefulness in sorption studies. *Environ. Chem. Lett.* **2009**, *7*, 79–84. [CrossRef]
26. Langmuir, I. The adsorption of gases on plane surfaces of glass, mica and platinum. *J. Am. Chem. Soc.* **1918**, *40*, 1361–1403. [CrossRef]
27. Freundlich, H.M.F. Über die Adsorption in Lösungen. *Z. Phys. Chem.* **1906**, *57*, 385–470. [CrossRef]
28. Lagergren, S. About the theory of so-called adsorption of soluble substances. *K. Sven. Vetenskapsakademiens Handl.* **1898**, *24*, 1–39.
29. Ho, Y.S.; McKay, G. Pseudo-second-order model for sorption processes. *Process Biochem.* **1999**, *34*, 451–465. [CrossRef]
30. Pighinelli, L.; Guimarães, M.F.; Becker, C.M.; Zehetmeyer, G.; Rasia, M.G.; Corria, D.S.; Paz, R.L.; Zannin, B.G.; Kmiec, M.; Tedesco, M.F.; et al. Structure and properties of nanocrystalline chitosan. *J. Appl. Biotechnol. Bioeng.* **2016**, *1*, 13–20. [CrossRef]
31. Kumar, D.; Kumar, P.; Pandey, J. Binary grafted chitosan film: Synthesis, characterization, antibacterial activity and prospects for food packaging. *Int. J. Biol. Macromol.* **2018**, *115*, 341–348. [CrossRef]
32. Bharathi, D.; Ranjithkumar, R.; Vasantharaj, S.; Chandarshekar, B.; Bhuvaneshwari, V. Synthesis and characterization of chitosan/iron oxide nanocomposite for biomedical applications. *Int. J. Biol. Macromol.* **2019**, *132*, 880–887. [CrossRef]
33. Baran, T.; Nasrollahzadeh, M. Pd/$CoFe_2O_4$/chitosan: A highly effective and easily recoverable hybrid nanocatalyst for synthesis of benzonitriles and reduction of 2-nitroaniline. *J. Phys. Chem. Solids* **2021**, *149*, 109772. [CrossRef]
34. Kumar-Krishnan, S.; Prokhorov, E.; Hernández-Iturriaga, M.; Mota-Morales, J.D.; Vázquez-Lepe, M.; Kovalenko, Y.; Sanchez, I.C.; Luna-Bárcenas, G. Chitosan/silver nanocomposites: Synergistic antibacterial action of silver nanoparticles and silver ions. *Eur. Polym. J.* **2015**, *67*, 242–251. [CrossRef]
35. Eddya, M.; Tbib, B.; El-Hami, K. A comparison of chitosan properties after extraction from shrimp shells by diluted and concentrated acids. *Heliyon* **2020**, *6*, e03486. [CrossRef]
36. Nasiri, A.; Rajabi, S.; Amiri, A.; Fattahizade, M.; Hasani, O.; Lalehzari, A.; Hashemi, M. Adsorption of tetracycline using $CuCoFe_2O_4$@chitosan as a new and green magnetic nanohybrid adsorbent from aqueous solutions: Isotherm, kinetic and thermodynamic study. *Arab. J. Chem.* **2022**, *15*, 104014. [CrossRef]
37. Atik, R.; Islam, R.; Ariza Gonzalez, M.; Chinwangso, P.; Lee, T.R. Recent advances in polymer-coated metal and metal oxide nanoparticles: From design to promising applications. *Nanomaterials* **2025**, *15*, 1744. [CrossRef]
38. Vohl, S.; Ban, I.; Stergar, J.; Slemnik, M. Synthesis, characterization, and application of magnetic zeolite nanocomposites: A review of current research and future applications. *Nanomaterials* **2025**, *15*, 921. [CrossRef]
39. Nga, N.K.; Thuy Chau, N.T.; Viet, P.H. Preparation and characterization of a chitosan/MgO composite for the effective removal of Reactive Blue 19 dye from aqueous solution. *J. Sci. Adv. Mater. Devices* **2020**, *5*, 65–72. [CrossRef]
40. Zhang, Z.; Lan, H.; Liu, H.; Qu, J. Removal of tetracycline antibiotics from aqueous solution by amino-Fe(III)-functionalized SBA-15. *Colloids Surf. A Physicochem. Eng. Asp.* **2015**, *471*, 133–138. [CrossRef]

41. Fan, B.; Tan, Y.; Wang, J.; Zhang, B.; Peng, Y.; Yuan, C.; Guan, C.; Gao, X.; Cui, S. Application of magnetic composites in removal of tetracycline through adsorption and advanced oxidation processes (AOPs): A review. *Processes* **2021**, *9*, 1644. [CrossRef]
42. Turan, B.; Sarigol, G.; Demircivi, P. Adsorption of tetracycline antibiotics using metal- and clay-embedded cross-linked chitosan. *Mater. Chem. Phys.* **2022**, *279*, 125781. [CrossRef]

Disclaimer/Publisher's Note: The statements, opinions and data contained in all publications are solely those of the individual author(s) and contributor(s) and not of MDPI and/or the editor(s). MDPI and/or the editor(s) disclaim responsibility for any injury to people or property resulting from any ideas, methods, instructions or products referred to in the content.